Construction and Building Materials 325 (2022) 126209

Contents lists available at ScienceDirect

Construction and Building Materials

journal homepage: www.elsevier.com/locate/conbuildmat

Effect of polymer binder on the mechanical and microstructural properties of pervious pavement materials

Yoonjae Shin [a], Hyeong Min Park [a], Jinha Park [a], Hongdong Cho [a], Seo-Eun Oh [b], Sang-Yeop Chung [b,*], Beomjoo Yang [a,*]

[a] School of Civil Engineering, Chungbuk National University, 1 Chungdae-ro, Seowon-gu, Cheongju 28644, Republic of Korea
[b] Department of Civil and Environmental Engineering, Sejong University, 209 Neungdong-ro, Gwangjin-gu, Seoul 05006, Republic of Korea

ARTICLE INFO

Keywords:
Pervious pavement materials
Polyurethane
Epoxy
Micro-CT analysis
Machine learning

ABSTRACT

Pervious pavements materials (PPMs) are prospective functional materials with the potential to make urban areas more environmentally friendly. In this study, the effects of polymer binders on the mechanical and microstructural properties of PPMs are analyzed experimentally and through machine learning. Polyurethane and epoxy, which are widely used due to their reasonable cost and high performance, are considered as polymer binders, and specimens with different aggregate size distributions are fabricated using these polymers. The mechanical properties of the specimens are analyzed using compressive and flexural strength tests, freeze–thaw durability tests, and water permeability tests. Then, the internal microstructure is characterized using micro-computed tomography, including the pore size distribution, pore sphericity, anisotropic ratios of the pores, pore tortuosity, and aggregate sphericity. The correlation between the mechanical properties and the pore structure is analyzed. The aggregate size distribution and the polymer viscosity affects the size of the internal pores, and thus the mechanical properties. Finally, machine learning is used to develop a model that can predict the microstructural properties and compressive strength of PPMs according to the aggregate size distribution and the properties of the polymer. The model was validated using experimental data, and the methods used in its creation could be used to derive a general model for PPMs.

1. Introduction

There is growing concern regarding abnormal weather and environmental pollution worldwide. As part of efforts to address these concerns, various studies have attempted to improve the functionality and stability of pavement surfaces in urban areas [1,2]. The durability of a permeable material can deteriorate due to freezing and thawing cycles [3,4]. This increases maintenance costs and can cause accidents as the surface breaks down [5–7]. Hence, there has been particular interest in the development of environmentally friendly and highly durable pavement materials.

'Greenness' describes the quality of not damaging the environment. Pervious pavement materials (PPMs) are functional materials with high feasibility that could be used to improve the greenness of urban areas [8]. In particular, PPMs with large pore structures reduce traffic noise and road surface heat, aid in water management such as recharging groundwater, and help to protect the local ecosystem. Sun et al. reported that increasing the size of the aggregate in PPMs increased the total porosity and water permeability, but decreased the compressive strength [9]. A similar study showed that decreasing the size of the aggregate increased the strength of the specimens [10]. Zhong and Wille showed that this strength enhancement was a result of an increase in the total bond area between neighboring aggregates [11]. In addition, Liu et al. investigated the correlation between the strength, permeability, and freeze–thaw durability of pervious concrete according to changes in the aggregate size and water–binder ratio. They showed that increasing the porosity improved the permeability, but decreased the overall mechanical performance [12]. Ćosić et al. also demonstrated that increasing the fine aggregate content improved the flexural strength of porous materials [13].

Conventional permeable pavements used in urban environments are generally fabricated using cement and asphalt binders, which have advantages in terms of cost and constructability. However, they have relatively poor abrasion resistance and load-bearing capacity due to the

* Corresponding authors.
E-mail addresses: sychung@sejong.ac.kr (S.-Y. Chung), byang@chungbuk.ac.kr (B. Yang).

https://doi.org/10.1016/j.conbuildmat.2021.126209
Received 29 July 2021; Received in revised form 20 December 2021; Accepted 22 December 2021

brittle nature of cement. Tire–road noise is also recognized as a major issue for porous concrete [14,15]. To address this, water-permeable pavements that use a polymer with high toughness and excellent environmental durability as a binder have been investigated. Recently, various high-performance polymers have been applied in the construction field at competitive prices, and this trend is expected to accelerate in future.

Lu et al. developed a polyurethane (PU) binder-based water permeable material and analyzed its dynamic response to pore water pressure. When the permeable material was subjected to cyclic loading, the pore water pressure was much larger than the pore air pressure, which was negligible [16,17]. Wang et al. studied the mechanical behavior of multiple-polymer–asphalt mixtures containing an anti-rutting agent, polyethylene, and styrene–butadiene styrene [18]. The energy consumption increased as the polymer content increased, but the multiple-polymer modified binder reduced fatigue. Lu et al. evaluated the environmental effect of cold mixing a polymer composite-based permeable pavement. PU binder-based pavements have high toughness and are environmentally friendly compared to stone mastic asphalt and conventional porous asphalt [19]. A bio-based PU binder containing recycled ceramic aggregate also developed as a permeable pavement material to help improve the environmental effects [20].

Extensive research has been conducted on the polymer-based pervious materials, and they have been successfully applied in various construction fields. However, the comprehensive understanding of these pervious materials is still restricted by the differences in polymers used in each research. Furthermore, there is still a lack of detailed research on internal structures and pore characteristics of PPMs. Therefore, it would be beneficial if the dependence of compressive strength/flexural strength, freeze–thaw resistance, and permeability coefficient on polymer type is systematically examined for a single well characterized system. In combination with experimental observations, computational interpretation will also help to gain a deeper understanding of the PPM and simultaneously develop its design rule.

Past studies have shown that the water permeability and mechanical characteristics of PPMs are greatly affected by the by the size of the aggregate. However, few studies have comprehensively analyzed the internal structure and mechanical performance of specimens with different binders. In this study, two types of binders, PU and epoxy, will be applied to a combination of aggregates, whose permeability was verified in other works, so that their characteristics can be analyzed. Fine aggregates will be incorporated into the specimens to control the internal voids and structures of the specimens. The compressive strength, flexural strength, freeze–thaw resistance, and permeability coefficient of each specimen will be measured, and the internal structure will be investigated using micro-computed tomography (CT). This will include analysis of the pore size distribution, pore sphericity, anisotropic ratios of the pores, pore tortuosity, and aggregate sphericity. In addition, a model based on machine learning will be proposed to predict the voids and compressive strengths of specimens according to the combination of aggregate and the properties of the polymer.

2. Methods

2.1. Materials

Epoxy and PU mortar binders were selected for the purpose of comparing the strength of PPM specimens. The aggregates consisted of size #2, #3, #6, and #8 silica sands with diameters of 2–5, 1–2, 0.2–0.4, and < 0.1 mm, respectively. Note that the smaller numbers indicate larger grains with a rougher surface. The particle size distribution of each aggregate is shown in Fig. 1. The PU binder consisted of a resin (HS-S100A, Hanseo Polymer Inc.) and a hardener (HS-S100B, Hanseo Polymer Inc.). The epoxy binder consisted of a resin and hardener (RM-200F, CheongWon chemical Co., Ltd.). The density and viscosity of the polymers are summarized in Table 1.

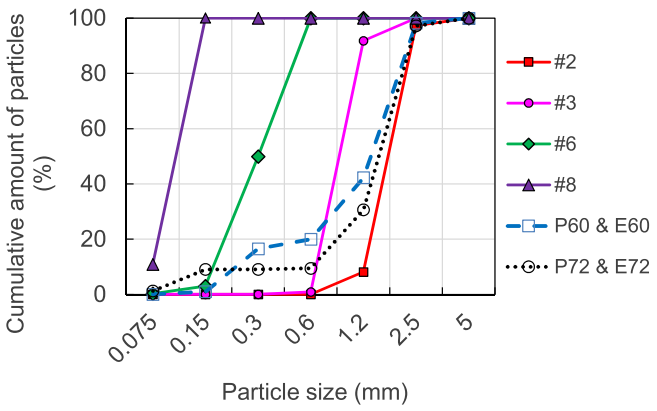

Fig. 1. Particle size distribution in aggregates and specimens.

Table 1
Density and viscosity of polymers.

Parameters	Value	
	PU (HS-S100AB)	Epoxy (RM-200F)
Density (g/cm^3)	1.05	1.21
Viscosity (cps)	1250	3000

The ratios of resin to hardener for the PU and epoxy were 1:2.36 and 4:1 by weight, respectively. The proportions of binder and aggregate were determined based on a previous study on PPMs, and they are shown in Table 2. Each specimen was labeled according to the type of binder and the mix ration of aggregate #2. Specifically, P and E indicate PU and epoxy, respectively, and 60 and 72 denote the weight ratio of aggregate #2 with respect to the total amount of aggregate. For example, P60 is a specimen composed of PU binder containing 60 wt% of aggregate #2. The binder to aggregate weight ratio (B/A) was set to 0.09% of the total amount of aggregate. The cumulative distributions of the aggregates in the specimens are shown in Fig. 1.

2.2. Experimental

The specimens were manufactured as follows. First, the aggregates were blended in a bowl for 3 min using a paddle mixer. Meanwhile, the resin and hardener for the binder were blended in another bowl for 1 min. Second, the blended binder was poured into the bowl containing the blended aggregates. The mixture of binder and aggregate was blended for 5 min. Third, the mixture was cast into molds for the compressive strength and freeze–thaw resistance tests (ϕ100 × 200 mm^3), flexural strength tests (150 × 150 × 700 mm^3), water permeability coefficient tests (300 × 300 × 65 mm^3), and micro-CT analysis (25 mm^3). Both the PU and epoxy PPM specimens were cured under ambient conditions for 3 d. Next, the specimens were demolded and cured under ambient conditions for another 4 d before they were used for the compressive, flexural, freeze–thaw, and water permeability tests.

Table 2
Mix ratios of PU- and epoxy-based PPMs.

Specimen	Mix ratio of aggregate				B/A[2]
	#2	#3	#6	#8	
P60	0.60	0.20	0.20	–	0.09
P72	0.72	0.18	–	0.09	
E60	0.60	0.20	0.20	–	
E72	0.72	0.18	–	0.09	

1. Range of aggregate size: #2 = 2–5 mm, #3 = 1–2 mm, #6 = 0.2–0.4 mm, #8 = < 0.1 mm.
2. Weight ratio of binder to aggregate (B/A). Ratio of resin to hardener was 4:1 by weight.

2.2.1. Compressive and flexural strength test

A universal testing machine (UTM, HST-200CS, Hanshin Kumpung Inc, Republic of Korea) with a load cell of 2000 kN was used for the compression and flexural tests [18,21]. The compression tests were conducted in accordance with ASTM C39. The flexural strength was measured using a four-point bending test in accordance with ASTM C78. In both tests, a strain rate of 1 mm/min was applied for the displacement control. The measured load (N) on each sample was converted to strength (MPa).

2.2.2. Freeze–thaw test

The freeze–thaw tests were conducted in accordance with ASTM C666. After curing, the specimens ($\phi 100 \times 200$ mm^3) were immersed in water for 4 d, then the surface was wiped dry. The specimens were placed in a rapid freeze–thaw test machine set to a temperature range of −20–20 °C. The freeze–thaw durability was estimated by measuring the compressive strength after 200 freeze–thaw cycles. The compressive strengths of the freeze–thaw specimens were divided by the normal compressive strength to calculate the reduction ratio.

2.2.3. Water permeability test

The water permeability coefficients of the PPM specimens were obtained in accordance with ASTM C1782. The specimens were fixed in the formwork and tightly sealed with rubber or sealing material to prevent water from leaking out of the block. Water was poured onto the upper side of the specimen until it overflowed, and the water level was adjusted to keep it constant. After measuring the amount of water that drained in 30 s, the permeability coefficient was calculated using the equation $K = (dQ)/(hAt)$. Here, K denotes the permeability coefficient (mm/s); d is the thickness of the specimen (mm); Q is the amount of runoff water (mm^3); h is the change in the water level (mm); A is the area of the specimen (mm^2); and t is the measurement time (30 s).

2.3. Microstructural characterization

In cement-based materials, particularly pervious materials, the pore structure is critical in determining the properties of the material. Several approaches can be used investigate the microstructure of a material, and micro-CT was selected to investigate the PPM specimens in this study. Micro-CT is a nondestructive method that can be used to visualize the inner structure of a target material without damaging the specimens [22–24]. It can also be used to examine the inside of pervious materials. Various standards for testing the permeability of construction materials have been published [25–27]; however, most of them relate to cement-based materials, and cases of quantitative analysis using CT are rare. In this study, various properties of the internal structures of the specimens were measured using micro-CT, and the effect of porosity on the mechanical properties of the polymer-based pervious materials was investigated.

Fig. 2 shows the imaging procedure used to visualize the pore structure, with specimen E72 as an example. In general, the 8-bit reconstructed micro-CT image consisted of a grayscale image with 256 values between 0 and 255, as shown in Fig. 2(a). For an effective investigation, a region of interest (ROI) was selected from the original image, which consisted of 1000 × 1000 pixels, each with a diameter of 16.03 μm (Fig. 2(b)). The ROI image was segmented into solid areas and pores by selecting an appropriate threshold value. The modified Otsu method [28] and manual selection were utilized to select this value. Fig. 2(c) shows a binarized image, where the white regions represent the pores and the black regions represent solid areas, such as the aggregates and binder. The pores were the main target of the micro-CT imaging, so the porous regions of each specimen were visualized in 3D by stacking a series of binary images. Fig. 2(d) shows a 3D image of the pores in specimen E72. Characteristics such as the porosity and pore size distribution can be examined using this image.

The permeable characteristics of the specimens, specifically the tortuosity, were also investigated using the volumetric pore images. Tortuosity τ is an index that describes the curvature of a pore path, which can be used to evaluate the connectivity and spatial heterogeneity of the pore distribution [29,30]. It can be defined as the ratio between the length of the curved path and the shortest distance between the target points. Fig. 3 shows a schematic diagram of the parameters used to determine the tortuosity. Here, L_{curve} denotes the actual distance of the curved path, and L_{short} is the minimum distance between the points. The A-star algorithm, a method of finding the minimum path between selected points, was used to compute L_{curve}. The details of this method were reported by Zeng and Church, and Chung et al. [31,32]. Once L_{curve} was computed, the tortuosity was obtained using the equation $\tau = L_{\text{curve}}/L_{\text{short}}$. The tortuosity of each specimen was examined using the volumetric pore image, and its correlation with these properties was investigated.

2.4. Machine learning model

Machine learning was used to predict the voids and compression strength of specimens according to the material formulation. A multi-gene genetic programming (MGGP)-based GPTIPS was adopted to identify correlations in the experimental data and drive model discovery [33,34]. GPTIPS is a technique based on the process of biological evolution, and it selects the optimal solution group through processes of selection, crossing, mutation, and substitution. The process of determining the optimal solution is performed repeatedly by selecting an

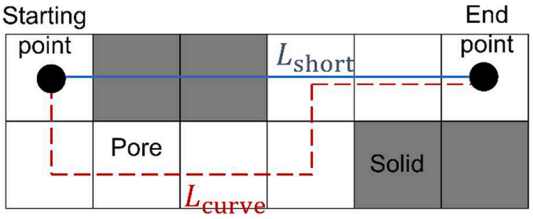

Fig. 3. Schematic of distances used to compute tortuosity where L_{curve} is the curved actual path, and L_{short} is the shortest distance between the target points.

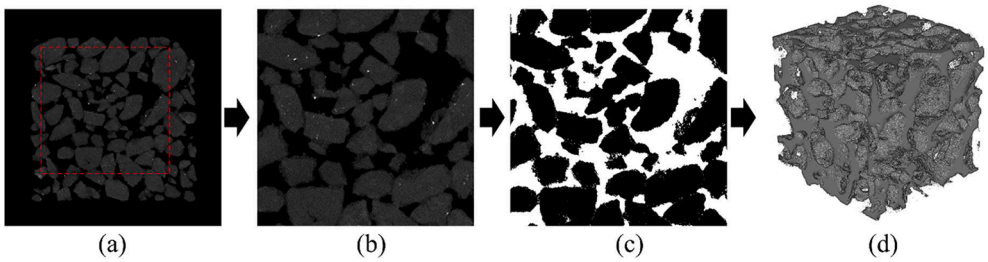

Fig. 2. Micro-CT imaging procedure with specimen E72 as an example. (a) Reconstructed micro-CT image, (b) region of interest (ROI), (c) binary image (black denotes solid regions and white denotes pore regions), and (d) 3D pore volume.

arbitrary value, then substituting some of the existing data according to its fitness. To prevent convergence to an incorrect value, mutations occur with a certain probability in the process of creating new values, thereby increasing diversity. The main parameters are the number of populations in one generation, and the selection of data that is crossed out to form the next generation. In this study, the number of populations in a generation was set to 150. The crossover for the next generation was constructed using the tournament method, and four objects were selected from the existing populations. This process was repeated 250 times to perform optimization.

The majority of studies on pervious materials have used classical continuum mechanics models to investigate the porosity–strength relationship. However, this makes it difficult to develop a unified constituent model for various PPMs because there are large variations in the data. In contrast, this study used an approach based on machine learning that was able to connect various defined inputs and outputs to derive an optimal correlation. The proposed model selects the most influential constants by assigning weights to the input data, and creates a model equation from these constants. This technique has the potential to derive a general model once sufficient data on the various constituents of PPMs have been accumulated. The MATLAB code used in the simulation is included in the supplementary information.

The machine learning was conducted in two stages. First, the MGGP model was used to estimate the volume fraction of the pores in the specimen by setting the input values to the average particle size and weight ratio of the aggregates, and the elastic modulus and viscosity of the polymer binders (Fig. 4(a)). The compressive strength of the specimen was then predicted based on the input variables with the porosity value added to the original input variables, as shown in Fig. 4(b). The validity of each analysis was verified by comparison with the micro-CT and compressive strength test results.

3. Results and discussion

3.1. Mechanical properties

Fig. 5(a) shows the compressive strength test results for each of the PPMs. In the specimens with PU binder, P72 had lower compressive strength than P60. In contrast, in the specimens with epoxy binder, E72 had higher compressive strength than E60. Moreover, both the specimens with epoxy binder had higher compressive strength than either of the specimens with PU binder. Despite containing the same combination of aggregates, the compressive strength of E60 was approximately 1.7 times higher than that of P60, and the compressive strength of E72 was approximately 4.5 times higher than that of P72.

The flexural strength test results showed no significant differences according to the polymer or aggregate type, as shown in Fig. 5(b). Specimens of P60 and E60 had the lowest and highest flexural strengths, respectively. However, these differences fell within the error range of the test, so it is difficult to conclude that there was a clear distinction between the samples. Fig. 5(c) shows the freeze–thaw test result. Freeze–thaw resistance can be defined as the compressive strength reduction ratio after the freeze–thaw test. Overall, the PU-based specimens were more vulnerable to freeze–thaw than the epoxy-based specimens.

The difference in the compressive strength of the specimens according to the type of binder can be attributed to the intrinsic properties of the polymers. According to the manufacturers (Hanseo Polymer Inc. and CheongWon chemical Co., Ltd.), the compressive strengths of PU and epoxy are 16 and 85 MPa, respectively; that is, the epoxy is approximately 5.3 times stronger than the PU. The significant difference in the compressive strength of the two polymers was reduced when they were mixed with aggregates. This is because the properties of the

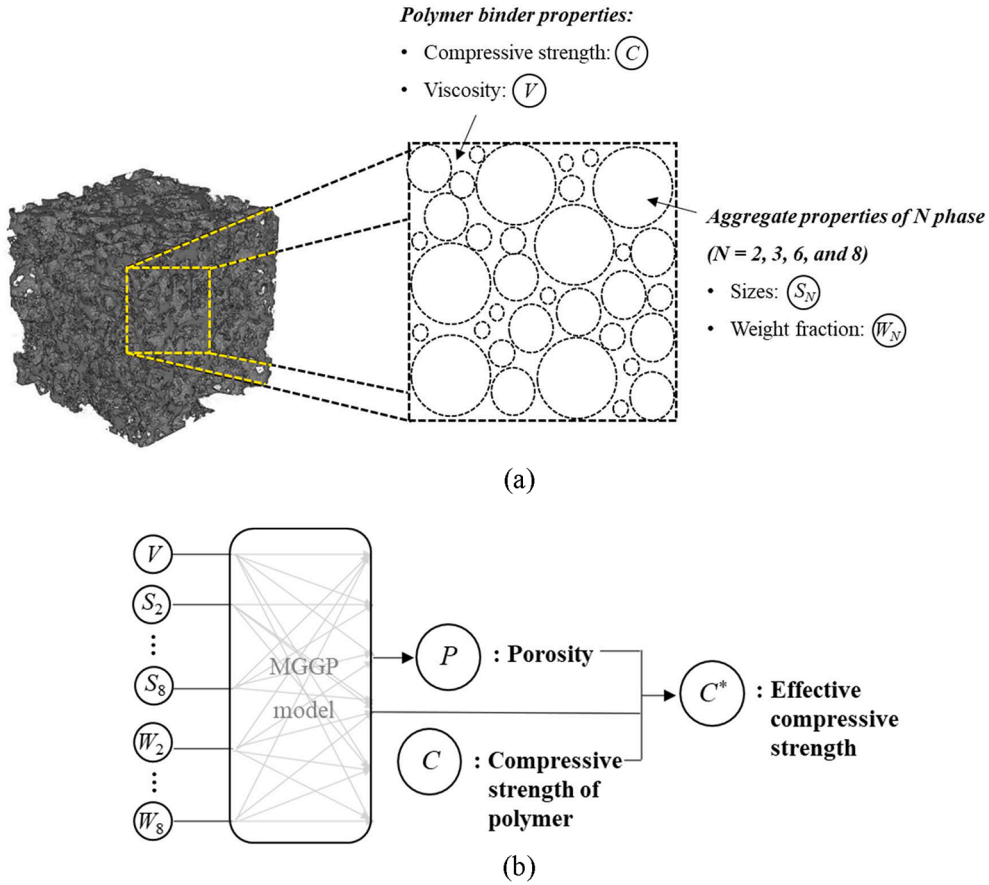

Fig. 4. Schematic illustrations of (a) input variables considered in the analysis and (b) the two steps of the machine learning model.

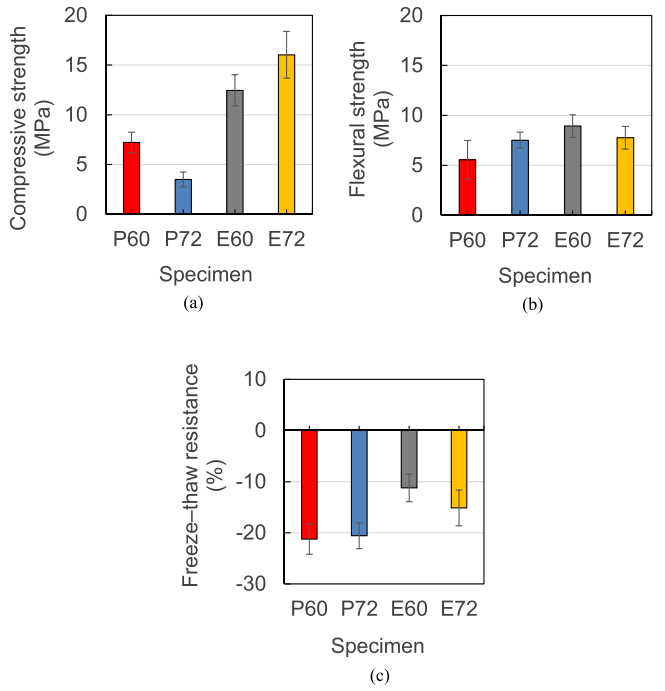

Fig. 5. (a) Compressive strength, (b) flexural strength, and freeze–thaw resistance results for the PU- and epoxy-based PPMs.

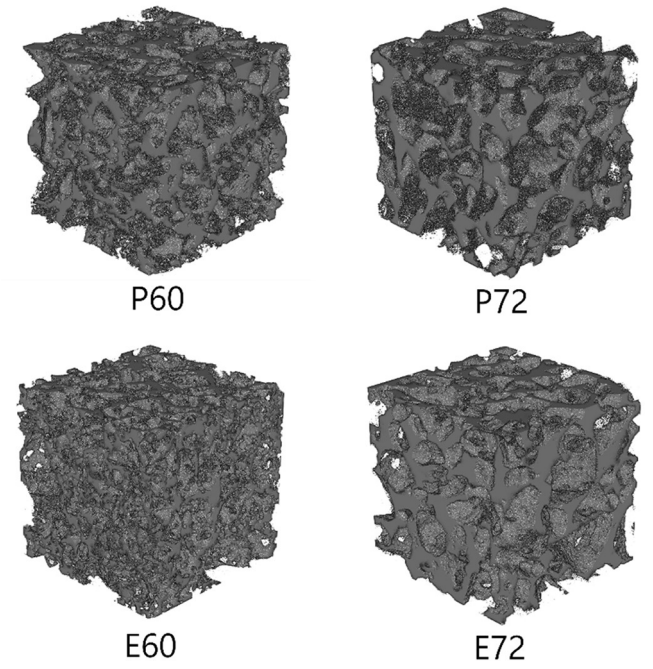

Fig. 6. Pore volume image for each specimen. The gray regions represent the pore paths within the specimens.

polymers were tempered when they were mixed with a relatively high volume of aggregate.

The viscosities of PU and epoxy at room temperature (~20 °C) were 1250 and 3000 cps, respectively, thus the viscosity of epoxy was approximately 2.4 times higher than that of PU. The mixing ratio of the resin and hardening materials was identical to that reported in the previous section. Lower viscosity is generally advantageous for the fabrication of composite materials [35,36]. However, in this study, the low viscosity polymer had an adverse effect on the compressive strength of the specimens. This is because the polymer was excessively well dispersed and formed relatively thin polymer chains between the aggregates [37]. Thus, a low-viscosity well-dispersed polymer can improve the integrity of the material, but it may not perform well in terms of energy absorption under compressive loading [38]. In addition, E72 was composed of coarser aggregates than E60, so the benefits of a low viscosity polymer may not have been exhibited clearly.

However, the low viscosity is thought to have had a positive effect on the flexural strength because the evenly distributed polymer chains inside the specimens helped to resist fractures caused by bending. Therefore, there was not as much difference in the flexural strength of the specimens with different polymers, compared to the compressive strength, as shown in Fig. 5(b). The freeze–thaw resistance showed a similar trend to the flexural strength. The PU-based specimens were vulnerable to freeze–thaw, and the epoxy-based specimens showed greater resistance. This is probably because the load applied to the specimen by freezing and thawing is closer to tension than compression, along with high mechanical properties inherent in the polymers.

3.2. Pore characteristics from micro-CT analysis

For cement-based materials, including pervious concrete, the pore structure is one of the most important factors in determining the material properties, such as the compressive strength and permeability. In this study, the pore characteristics of the samples were investigated using micro-CT data. Fig. 6 shows an illustration of the pores in each specimen. Only pores larger than 32 μm were considered owing to pixel (or voxel) size used.

As shown, each case contained dominant pore networks that passed through the entire specimen, and numerous locally dispersed pores were also found visually and statistically. For a quantitative investigation, the porosity of the specimens was evaluated using the number of pore voxels within the samples. The computed porosities of specimens P60, P72, E60, and E72 were 32.03%, 31.01%, 31.08%, and 29.61%, respectively. All the specimens had similar porosity, although E72 had slightly lower porosity than the other specimens. This indicates that the pore volume is not a critical factor in the compressive strength of the specimens, and other characteristics should be considered to determine the correlation with the mechanical properties.

In addition to the porosity, the pore size distribution of the specimens was examined. Fig. 7 shows the pore size distribution for each specimen. Large pore clusters penetrating the specimens were not considered, and only local pores were included. The figure shows the relative difference in the pore size characteristics of each material. In the PU-based specimens, P72 contained larger pores than P60, which could be responsible for its lower compressive strength, as shown in Fig. 5. Conversely, in the epoxy-based specimens, E72 had a higher proportion of small pores than E60, which may account for its relatively high compressive strength.

For a more detailed investigation of the pore characteristics, the pore shape was also investigated. Wadell's sphericity, an index that describes the degree of equiaxed shape, was used to characterize the pore shape quantitatively. It is defined as the ratio between the surface area of a target pore and the surface area of a sphere with the same volume as the pore [39]. The sphericity has a value between 0 and 1, where a value of 1 indicates a pore that is perfectly spherical. As with the pore size distribution, only locally dispersed pores were considered. Fig. 8 shows the sphericity of the pores in each material. Among the specimens, P72 had a higher proportion of more anisotropic pores than the other specimens, which may account for its lower compressive strength [40]. Among the epoxy-based specimens, E72 had a higher proportion of pores with a sphericity of 1; that is, specimen E60 had greater anisotropy, which could reduce the compressive strength.

In addition to the sphericity, the anisotropic ratio of each pore was examined. The anisotropic ratio was defined as the ratio between the maximum and minimum principal axes of the pores. The anisotropy ratio can have values greater than 1, and a value of 1 denotes an

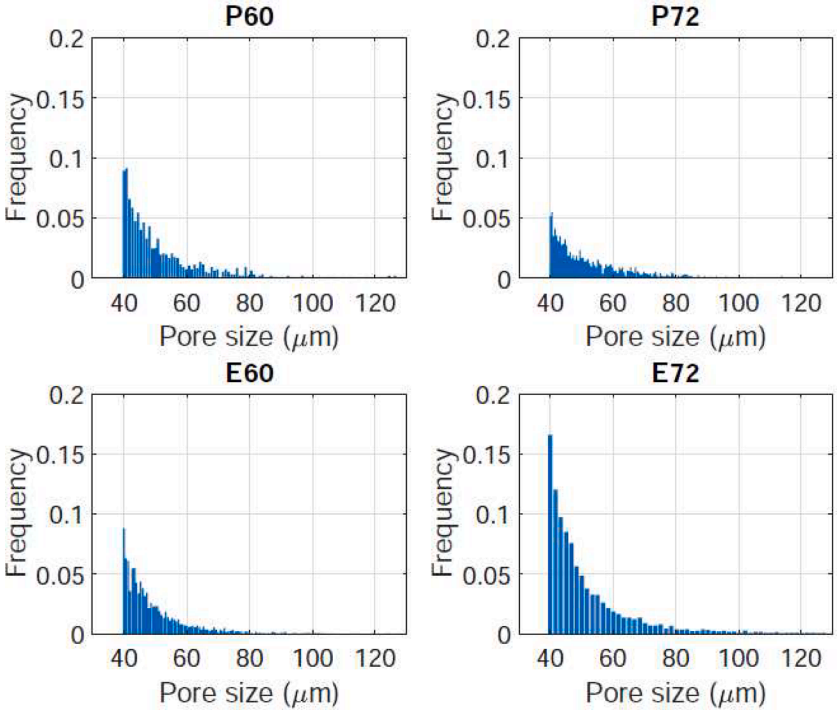

Fig. 7. Pore size distribution in each specimen. Only pores greater than 32 μm were included, and large pore clusters penetrating the specimen were not considered.

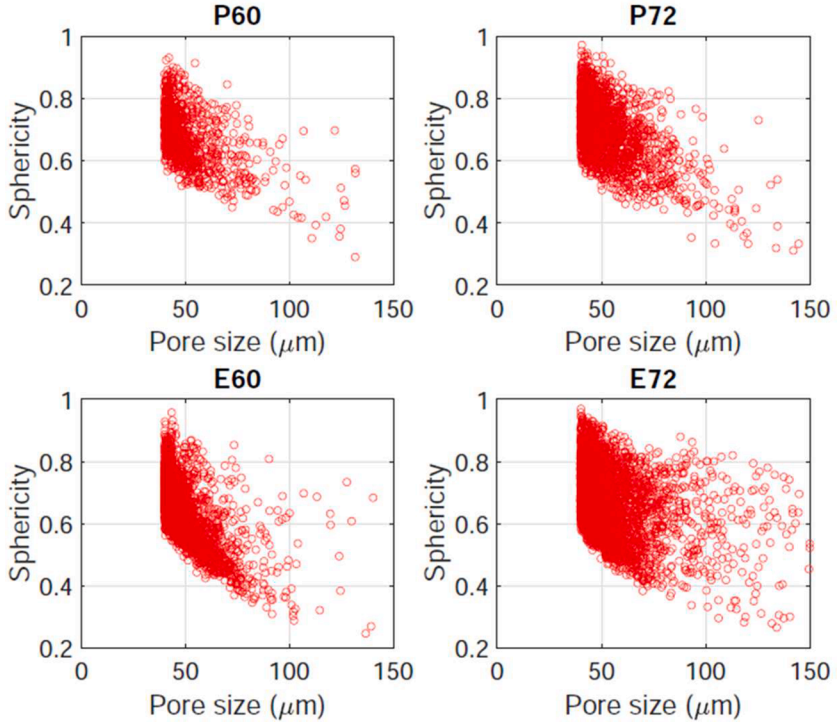

Fig. 8. Sphericity of pores within the specimens. (Sphericity of 1 denotes a completely spherical pore.)

isotropic pore. Fig. 9 shows the anisotropic ratio of the specimens. As with sphericity, P72 contained a greater proportion of pores with a high anisotropic ration than the other specimens. Compared to the PU-based specimens, the epoxy-based specimens with the same mix proportions tended to have a lower anisotropic ratio. This indicated that the epoxy-based specimens contained relatively isotropic pores, which improve the mechanical properties, and the anisotropic ratios show the same trends as sphericity.

The sphericity of the aggregate particles was also investigated, as shown in Fig. 10. The sphericity of the aggregates in the PU- and epoxy-based specimens were similar, and in each case the 72-series specimens had slightly larger sphericity values. In particular, the aggregates in specimen P72 had a slightly higher proportion of relatively low (<0.4) sphericity, which contributes to the aforementioned anisotropic pores of the specimen.

The permeable characteristics, specifically the tortuosity, were also

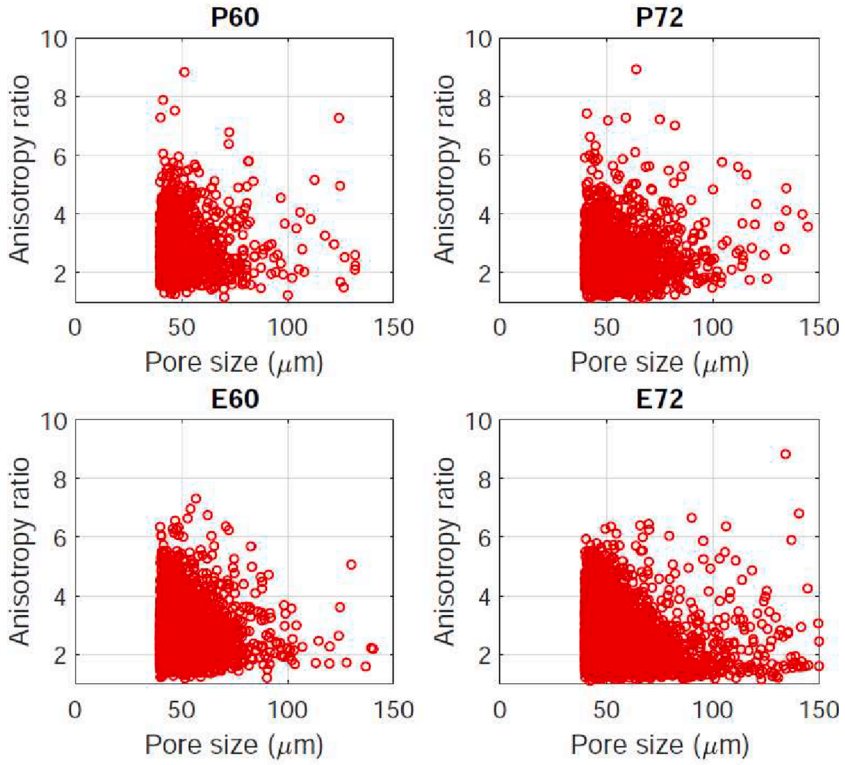

Fig. 9. Anisotropic ratios of pores within the specimens. (The minimum value of the anisotropic ratio is 1, and it indicates a pore that is completely isotropic.)

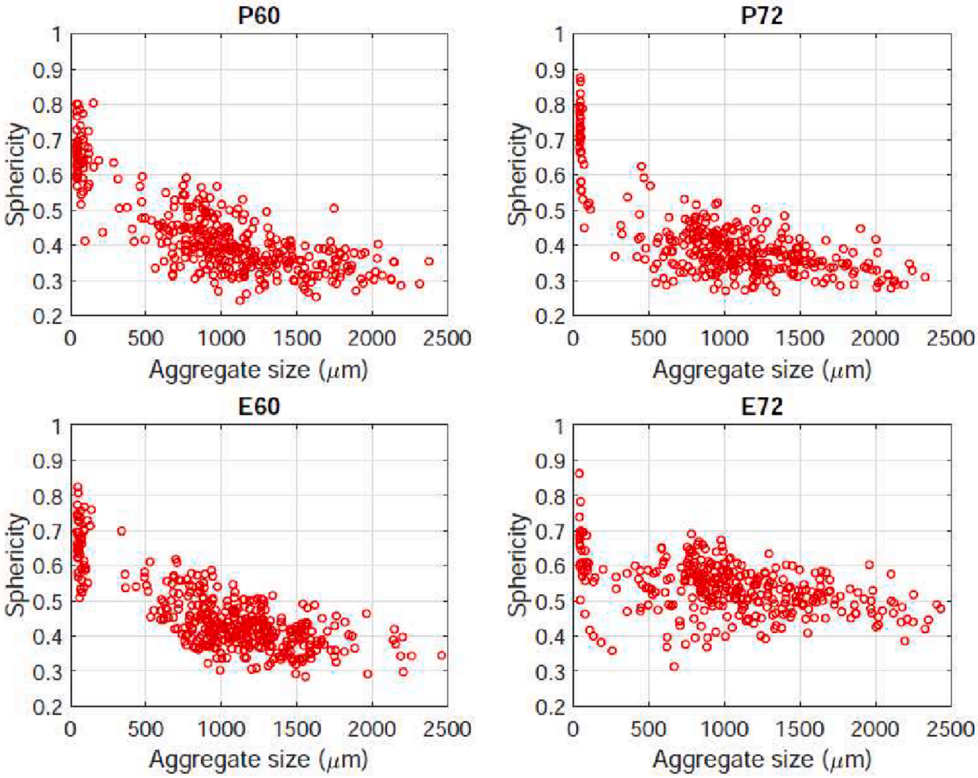

Fig. 10. Sphericity of aggregates within the specimens (Sphericity of 1 denotes completely spherical aggregate.)

evaluated using the micro-CT data. Tortuosity can be used as an index to describe the complexity of the pore channel where the minimum value is 1, which denotes approximately straight pores, and higher values indicate more complex pore structures. The results for the specimens are shown in Fig. 11. All the specimens showed similar general trends, but the relative frequency differed slightly. The PU-based specimens had

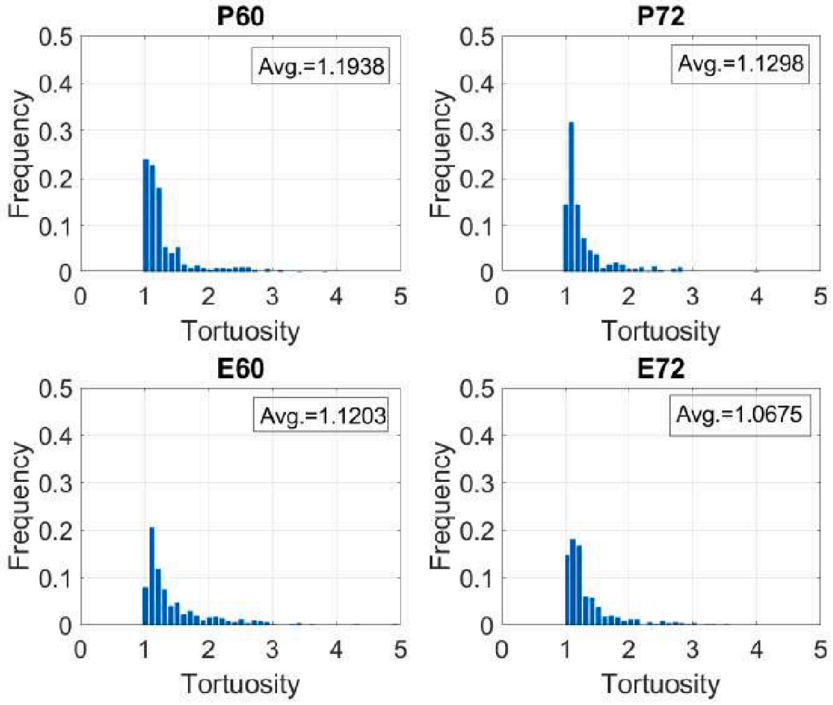

Fig. 11. Tortuosity distribution of each specimen.

slightly higher tortuosity than the epoxy-based specimens, which indicates that the curvature was more complex. In both the PU- and epoxy-based specimens, the distribution and average value of the tortuosity tended towards higher values in the 60-series specimens than the 72-series specimens. This was mainly due to the difference in the size of the aggregates. Among the specimens, E72 was considered to have superior permeable characteristics as it contained a higher proportion of relatively low tortuosity pores. In general, higher tortuosity indicates a longer pore path, which reduces the compressive strength [41]. Accordingly, the tortuosity results in this study closely coincide with the trends in compressive strength.

Overall, the characteristics observed using micro-CT, including the pore size distribution, pore shape, and tortuosity, consistently showed that specimen E72 had the most desirable properties in terms of pore structure. This correlated with the compressive strength, which also confirms that the relative strength can be predicted from the detailed pore characteristics. The permeability coefficients for specimens E60, E72, P60, and P72 were 0.4, 0.9, 0.6, and 2.2 mm/s, respectively. As with the CT analysis, specimen E72 was found to have the highest permeability. In addition, the permeability coefficient of P72 was more than twice that of P60. Thus, it could be concluded that the combination of aggregates in the 72-series specimens is advantageous in terms of the permeability performance of PPMs.

3.3. Machine learning simulation results

For permeable materials, the internal porosity ratio affects the overall performance of the material, but it is quite difficult to measure quantitatively. This study attempted to derive a model based on the viscosity of the polymer *V,* the weight ratio of the aggregates *W*, and the mean aggregate size *S*. For *W* and *S*, the values corresponding to each aggregate (#2, 3, 6, and 8) are indicated with subscripts. For example, W_6 denotes the weight fraction of aggregate #6 in the specimen, and S_3 denotes the mean particle size in aggregate #3, which was 1.5 mm. A model equation with more variables can improve the precision of the results, but there is a concern that the equation may become complicated and difficult to use [42]. Hence, the most influential factors were selected for use in the adopted GPTIPS approach, and terms with less influence were excluded. It was determined that *V*, W_2, and W_8 had the greatest effect on the void, and a model based on machine learning was derived. This is given by the equation

$$P = 0.34 - 0.02W_2 - 8.8\cdot10^{-5}\left(\sqrt{W_2} - VW_2W_8\right) - 5.7\cdot10^{-6}V \quad (1)$$

where *P* indicates the volume fraction of the internal pores, *V* denotes the viscosity of polymer binder, and W_2 and W_8 are the weight fractions of aggregates *#2* and #8, respectively. Although $S_{2,\ 3,\ 6,\ 8}$ and $W_{3,\ 6}$ were initially applied as input values, they were excluded from the final expression. This is because their effects were relatively insignificant compared to the other factors, so they were removed to make the model formulation more concise.

The most distinguishing feature of pervious materials was considered to be their high porosity compared to other materials, so this was selected as the main factor for the simulation. An equation for predicting the compressive strength of a specimen was then established by adding a porosity term to the compressive strength of the polymer. This gave the expression

$$C^* = 731.5P - 79.7W_8 + 0.18C - 230.4 \quad (2)$$

where *C** denotes the compressive strength of the specimen. Fig. 12 (a) shows a comparison between the compressive strength values predicted by Eq. (2) and the experimental results. There was a fairly high degree of regularity in this experiment, which resulted in good agreement. Based on Eq. (2), the results for additional conditions that were not tested previously (C = 10, 50, and 90 MPa; V = 1000, 2000, and 3000 cps) were predicted, as shown in Fig. 12(b). When a polymer binder with high compressive strength was used, the effective compressive strength of the pervious specimen increased. In addition, the rate of increase was greater between the relatively low and intermediate levels, than between the intermediate and high levels. As the viscosity increased, the strength decreased, but the effect was insignificant. This is considered to be a limitation of this study, in that experiments were not performed using polymers with different viscosities.

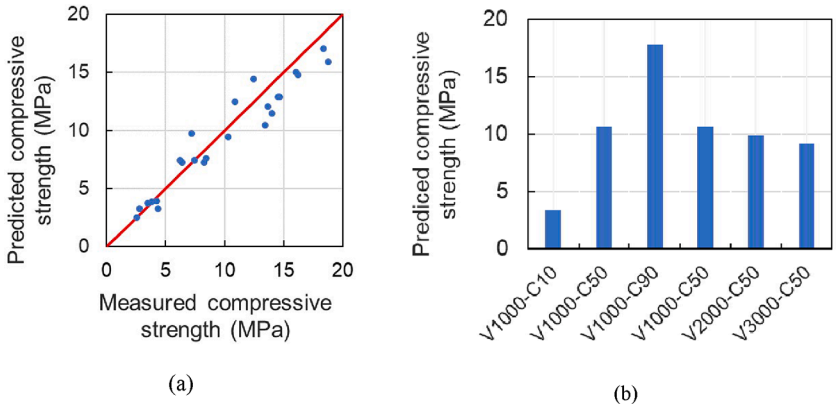

(a) (b)

Fig. 12. (a) Machine learning predictions for the compressive strength of the specimens and (b) parametric predictions with higher T and P values.

3.4. Comparisons with literatures

The results of this study are shown in Table 3. There were no prior studies that comprehensively tested the compressive, flexural, freeze–thaw, and permeability properties of pervious materials. However, for comparison, the results of similar studies are also presented. The majority of the existing studies tested the compressive and flexural strength of pervious materials, and the freeze–thaw resistance and permeability coefficients were sometimes investigated. In this study, the compressive strength of the epoxy-based specimens was lower than that reported elsewhere, but the flexural strength was higher. This is probably due to the inherent high tensile strength of the polymer binders [43]. The freeze–thaw durability results were similar to those reported elsewhere.

According to ASTM C1701, the minimum permeability coefficient that guarantees water permeability is 1.5 mm/s, and it is necessary to achieve a value greater than this criterion [44]. However, other performance characteristics could vary according to the application, and no clear criteria are given. The Republic of Korea requires a compressive strength of at least 10 MPa for pervious pavements applied to sidewalks, and at least 15 MPa for bicycle paths and parking lots [45]. In addition, for cement-based permeable paving materials applied to construction sites in Korea, a flexural strength of at least 2 MPa and coefficient of slip resistance of at least 40 are required. As shown in Table 3, most of the indicators exceed these requirements, and the flexural strength of the specimen is significantly improved. Based on the overall test results, the proposed specimens could soon be applied in industrial fields once the price becomes competitive and the manufacturing process is optimized. The experimental results in this study indicate that E72 may have the highest field applicability among the four candidate groups. Moreover, E72 has a high coarse aggregate content (#2), so it is also expected to have excellent water permeability and manufacturability.

4. Conclusions

Experimental and computational investigations of epoxy- and PU-based PPMs were conducted in this study. A series of compressive strength, flexural strength, freeze–thaw durability, and permeability tests were carried out in accordance with the relevant standards, and the experimental data were applied to machine learning. From this, the following conclusions can be drawn:

(1) The volume fraction of pores in the polymer-based PPMs was 29–31%.
(2) Compared to the PU-based PPM, the compressive strength of the epoxy-based PPM was approximately 2.6 times higher, and the flexural strength was approximately 1.5 times higher.
(3) The aggregate combination and polymer viscosity affect the size and shape of the internal pores, and a large number of small spherical pores were formed in specimen E72. It is believed that this affected the mechanical properties of E72.
(4) A machine learning model considering various material constituents was applied, and the effectiveness of the model was validated by using experimental data.

Machine learning simulations perform better with large amounts of data, and the amount of training data in this study was relatively small, reflecting a limitation of this work. However, although the amount of data was insufficient, the techniques presented could be used to derive a general model, once a sufficient amount of data on PPMs have been accumulated. The proposed framework is versatile, and it is expected to be applied to various pervious materials. However, the machine learning model should be compared with additional experimental studies considering different types of polymers, aggregate combinations, and

Table 3
Test results for PPM specimens and comparison with other studies.

Binder	Compressive strength (MPa)	Flexural strength (MPa)	Freeze–thaw resistance* (%)	Permeability coefficient(mm/s)	Reference
PU (P60)	7.21	5.35	−21.24	0.4	Present
PU (P72)	3.49	7.71	−20.57	0.9	study
Epoxy (E60)	12.45	9.03	−11.22	0.6	
Epoxy (E72)	16.03	7.46	−15.15	2.2	
Cement + styrene-butadiene	24.5	4.2	−13	–	[46]
Cement + vinyl-acetate	50	5.1	−10	–	[46]
Cement + butyl styrene	20.76	–	–	0.54	[47]
Cement + polyvinyl	19.8	–	–	0.43	[47]
PU	6.2	–	–	8	[20]
Styrene butadiene rubber	9.3	2.3	–	–	[48]
Vinyl acetate ethylene + acrylic emulsion	36	5.5	–	–	[49]

*Compressive strength reduction ratio after freeze–thaw test.

test conditions for more reliable predictions. This will be explored in future works.

CRediT authorship contribution statement

Yoonjae Shin: Writing – original draft, Conceptualization. **Hyeong Min Park:** Data curation, Investigation. **Jinha Park:** Data curation. **Hongdong Cho:** Formal analysis. **Seo-Eun Oh:** Formal analysis. **Sang-Yeop Chung:** Methodology, Formal analysis. **Beomjoo Yang:** Writing – review & editing, Supervision.

Declaration of Competing Interest

The authors declare that they have no known competing financial interests or personal relationships that could have appeared to influence the work reported in this paper.

Acknowledgements

This work was supported by grants from the National Research Foundation (NRF) of Korea funded by the Korean government (MSIT) (2020R1C1C1005063 and NRF-2021R1A4A3030924). In addition, this work was financially supported by the Ministry of the Interior and Safety through the Human Resource Development Project in Earthquake Disaster Management.

References

[1] E.J. Gago, J. Roldan, R. Pacheco-Torres, J. Ordóñez, The city and urban heat islands: A review of strategies to mitigate adverse effects, Renew. Sustain. Energy Rev. 25 (2013) 749–758.
[2] N. Xie, M. Akin, X. Shi, Permeable concrete pavements: A review of environmental benefits and durability, J. Cleaner Prod. 210 (2019) 1605–1621.
[3] S. Badeli, A. Carter, G. Doré, S. Saliani, Evaluation of the durability and the performance of an asphalt mix involving Aramid Pulp Fiber (APF): Complex modulus before and after freeze-thaw cycles, fatigue, and TSRST tests, Constr. Build. Mater. 174 (2018) 60–71.
[4] B. Richardson, Defects and Deterioration in Buildings: A Practical Guide to the Science and Technology of Material Failure, Routledge, 2002.
[5] H. Wu, J. Yu, W. Song, J. Zou, Q. Song, L. Zhou, A critical state-of-the-art review of durability and functionality of open-graded friction course mixtures, Constr. Build. Mater. 237 (2020), 117759.
[6] M.A. Ahammed, S.L. Tighe, Concrete pavement surface textures and multivariables frictional performance analysis: a North American case study, Can. J. Civ. Eng. 35 (7) (2008) 727–738.
[7] L.N. Antunes, E. Ghisi, L.P. Thives, Permeable pavements life cycle assessment: A literature review, Water 10 (11) (2018) 1575.
[8] C. Plati, Sustainability factors in pavement materials, design, and preservation strategies: A literature review, Constr. Build. Mater. 211 (2019) 539–555.
[9] Z. Sun, X. Lin, A. Vollpracht, Pervious concrete made of alkali activated slag and geopolymers, Constr. Build. Mater. 189 (2018) 797–803.
[10] J. Yang, G. Jiang, Experimental study on properties of pervious concrete pavement materials, Cem. Concr. Res. 33 (3) (2003) 381–386.
[11] R. Zhong, K. Wille, Compression response of normal and high strength pervious concrete, Constr. Build. Mater. 109 (2016) 177–187.
[12] H. Liu, G. Luo, L. Wang, W. Wang, W. Li, Y. Gong, Laboratory evaluation of eco-friendly pervious concrete pavement material containing silica fume, Applied Sciences 9 (1) (2019) 73.
[13] K. Ćosić, L. Korat, V. Ducman, I. Netinger, Influence of aggregate type and size on properties of pervious concrete, Constr. Build. Mater. 78 (2015) 69–76.
[14] D.e. Chen, C. Ling, T. Wang, Q. Su, A. Ye, Prediction of tire-pavement noise of porous asphalt mixture based on mixture surface texture level and distributions, Constr. Build. Mater. 173 (2018) 801–810.
[15] P. Mikhailenko, Z. Piao, M.R. Kakar, M. Bueno, S. Athari, R. Pieren, K. Heutschi, L. Poulikakos, Low-Noise pavement technologies and evaluation techniques: A literature review, Int. J. Pavement Eng. (2020) 1–24.
[16] G. Lu, T. Törzs, P. Liu, Z. Zhang, D. Wang, M. Oeser, J. Grabe, Dynamic Response of Fully Permeable Pavements: Development of Pore Pressures under Different Modes of Loading, J. Mater. Civ. Eng. 32 (7) (2020) 04020160.
[17] G. Lu, H. Wang, Y. Zhang, P. Liu, D. Wang, M. Oeser, J. Grabe, The hydro-mechanical interaction in novel polyurethane-bound pervious pavement by considering the saturation states in unbound granular base course, Int. J. Pavement Eng. (2021) 1–14.
[18] J. Wang, J. Yuan, F. Xiao, Z. Li, J. Wang, Z. Xu, Performance investigation and sustainability evaluation of multiple-polymer asphalt mixtures in airfield pavement, J. Cleaner Prod. 189 (2018) 67–77.
[19] G. Lu, Y. Wang, H. Li, D. Wang, M. Oeser, The environmental impact evaluation on the application of permeable pavement based on life cycle analysis, Int. J. Transp. Sci. Technol. 8 (4) (2019) 351–357.
[20] G. Lu, P. Liu, Y. Wang, S. Faßbender, D. Wang, M. Oeser, Development of a sustainable pervious pavement material using recycled ceramic aggregate and bio-based polyurethane binder, J. Cleaner Prod. 220 (2019) 1052–1060.
[21] B. Rabia, T.H. Daouadji, R. Abderezak, Effect of air bubbles in concrete on the mechanical behavior of RC beams strengthened in flexion by externally bonded FRP plates under uniformly distributed loading, 1 3(1) (2021) 41.
[22] N. Bossa, P. Chaurand, J. Vicente, D. Borschneck, C. Levard, O. Aguerre-Chariol, J. Rose, Micro-and nano-X-ray computed-tomography: A step forward in the characterization of the pore network of a leached cement paste, Cem. Concr. Res. 67 (2015) 138–147.
[23] S.-Y. Chung, J.-S. Kim, D. Stephan, T.-S. Han, Overview of the use of micro-computed tomography (micro-CT) to investigate the relation between the material characteristics and properties of cement-based materials, Constr. Build. Mater. 229 (2019), 116843.
[24] R. Benferhat, T.H. Daouadji, R. Abderezak, Effect of porosity on fundamental frequencies of FGM sandwich plates, 1 3(1) (2021) 25.
[25] PA (2014).
[26] A. C/CM-09, Standard Test Method for Infiltration Rate of in-Place Pervious Concrete, (2009).
[27] ACI 522R-10, Report on Pervious Concrete, Ameri. Concre. Institute. (2010).
[28] S.-Y. Chung, P. Sikora, D. Stephan, M., Abd Elrahman, The effect of lightweight concrete cores on the thermal performance of vacuum insulation panels, Materials 13 (11) (2020) 2632.
[29] R. Zhong, M. Xu, R. Vieira Netto, K. Wille, Influence of pore tortuosity on hydraulic conductivity of pervious concrete: Characterization and modeling, Constr. Build. Mater. 125 (2016) 1158–1168.
[30] K.M. Graczyk, M. Matyka, Predicting porosity, permeability, and tortuosity of porous media from images by deep learning, Sci. Rep. 10 (1) (2020) 1–11.
[31] W. Zeng, R.L. Church, Finding shortest paths on real road networks: the case for A, International journal of geographical information science 23 (4) (2009) 531–543.
[32] S.-Y. Chung, T.-S. Han, S.-Y. Kim, Reconstruction and evaluation of the air permeability of a cement paste specimen with a void distribution gradient using CT images and numerical methods, Constr. Build. Mater. 87 (2015) 45–53.
[33] R.C. Eberhart, Y. Shi, Computational intelligence: concepts to implementations, Elsevier, 2011.
[34] A.H. Gandomi, E. Atefi, Software review: the GPTIPS platform, Genet. Program Evolvable Mach. 21 (1) (2020) 273–280.
[35] C.B. Kim, K.B. Jeong, B.J. Yang, J.-W. Song, B.-C. Ku, S. Lee, S.-K. Lee, C. Park, Facile supramolecular processing of carbon nanotubes and polymers for electromechanical sensors, Angew. Chem. Int. Ed. 56 (51) (2017) 16180–16185.
[36] S.Y. Kim, J.-u. Jang, B.F. Haile, M.W. Lee, B. Yang, Swarm intelligence integrated micromechanical model to investigate thermal conductivity of multi-walled carbon nanotube-embedded cyclic butylene terephthalate thermoplastic nanocomposites, Compos. A Appl. Sci. Manuf. 128 (2020) 105646, https://doi.org/10.1016/j.compositesa:2019.105646.
[37] J. Cho, H.G. Jang, S.Y. Kim, B. Yang, Flexible and coatable insulating silica aerogel/polyurethane composites via soft segment control, Compos. Sci. Technol. 171 (2019) 244–251.
[38] J. Cho, S.-K. Lee, S.-H. Eem, J.G. Jang, B. Yang, Enhanced mechanical and thermal properties of carbon fiber-reinforced thermoplastic polyketone composites, Compos. A Appl. Sci. Manuf. 126 (2019) 105599, https://doi.org/10.1016/j.compositesa:2019.105599.
[39] J.W. Bullard, E.J. Garboczi, Defining shape measures for 3D star-shaped particles: Sphericity, roundness, and dimensions, Powder Technol. 249 (2013) 241–252.
[40] S.-Y. Chung, D. Stephan, M.A. Elrahman, T.-S. Han, Effects of anisotropic voids on thermal properties of insulating media investigated using 3D printed samples, Constr. Build. Mater. 111 (2016) 529–542.
[41] R. Song, L. Zheng, Y. Wang, J. Liu, Effects of pore structure on sandstone mechanical properties based on micro-CT reconstruction model, Advances in Civil Engineering 2020 (2020) 1–21.
[42] J. Jung, C. Park, G.J. Yun, A thermophysically balanced multiscale coarse-grained potential for glass-forming polymers with the energy renormalization method, Functional Composites and Structures 3 (1) (2021) 015006, https://doi.org/10.1088/2631-6331/abe6b0.
[43] B.J. Yang, B.R. Kim, H.K. Lee, Micromechanics-based viscoelastic damage model for particle-reinforced polymeric composites, Acta Mech. 223 (6) (2012) 1307–1321.
[44] D.R. Smith, K. Earley, J.M. Lia, Potential application of ASTM C1701 for evaluating surface infiltration of permeable interlocking concrete pavements, in: H.J. Brown, M. Offenberg (Eds.), Pervious Concrete, ASTM International, 100 Barr Harbor Drive, PO Box C700, West Conshohocken, PA 19428-2959, 2012, pp. 1–9, https://doi.org/10.1520/STP104560.
[45] E.-J. Ko, E.-J. Goh, H.-J. Seok, S.-H. Lee, A study of developing guides for the construction site quality control of porous concrete, Journal of the Korea Institute of Building Construction 9 (3) (2009) 65–71.
[46] F. Giustozzi, Polymer-modified pervious concrete for durable and sustainable transportation infrastructures, Constr. Build. Mater. 111 (2016) 502–512.
[47] F.C. Shen, Y.X. Zhou, Z.D. Li, W.L. Shi, Study on mechanical properties of polymer pervious cement concrete, IOP Conference Series: Materials Science and

Engineering, IOP Publishing 479 (2019) 012091, https://doi.org/10.1088/1757-899X/479/1/012091.
[48] T.M. Borhan, Z. Kammouna, Enhancing physical and mechanical properties of pervious concrete, AIP Conference Proceedings, AIP Publishing LLC (2020), 020098.
[49] Y.u. Chen, K. Wang, X. Wang, W. Zhou, Strength, fracture and fatigue of pervious concrete, Constr. Build. Mater. 42 (2013) 97–104.